Physical Communication 31 (2018) 87–95

Contents lists available at ScienceDirect

Physical Communication

journal homepage: www.elsevier.com/locate/phycom

Full length article

3D-OMP and 3D-FOMP algorithms for DOA estimation

Keyvan Aghababaiyan [a,*], Reza Ghaderi Zefreh [b], Vahid Shah-Mansouri [a]

[a] School of Electrical and Computer Engineering, College of Engineering, University of Tehran, Tehran, Iran
[b] Department of Electrical and Electronic Engineering, Isfahan University of Technology, Isfahan, Iran

ARTICLE INFO

Article history:
Received 19 June 2018
Accepted 19 October 2018
Available online 30 October 2018

Keywords:
Direction of arrival (DoA)
Three dimensional orthogonal matching pursuit
Adaptive antennas

ABSTRACT

Adaptive antennas and antenna array processing have vital effects on enhancing the performance of wireless communication networks. One of the most significant applications of adaptive antenna systems is the Direction of Arrival (DOA) detection. Several schemes have been proposed in the literature for DOA estimation in two-dimensional space. Among them, Orthogonal Matching Pursuit (OMP) algorithm provides several advantages in comparison to other schemes. The OMP algorithm reduces complexity and improves resolution of detection. Furthermore, in this algorithm, the number of signal emitters is not required to be known. In this paper, we extend the OMP algorithm and propose Three Dimensional OMP (3D-OMP) scheme for DOA estimation in three dimensional space. We provide a redundant dictionary for 3D-OMP scheme by employing azimuth and elevation angles. Simulation results show the high performance of the 3D-OMP algorithm when the signal to noise ratio is higher than $-10dB$. Moreover, the 3D-OMP algorithm has a high efficiency in detecting multiple signal sources, simultaneously. Then, we evaluate the accuracy of the estimated directions by the 3D-OMP algorithm via comparing the variance of estimation error with the Cramer-Rao bound. Nevertheless, DOA estimation by the 3D-OMP algorithm has a substantial challenge where it cannot distinguish between two adjacent signal sources. To resolve this challenge, we propose Three Dimensional Focused Orthogonal Matching Pursuit (3D-FOMP) algorithm. The 3D-FOMP algorithm is an improved version of the 3D-OMP algorithm. It can detect two adjacent signal sources when the beam former has a single peak corresponding to a direction between right directions. In addition, we show the 3D-OMP and 3D-FOMP algorithms have lower complexities in comparison to the 3D-MUSIC and 3D-ESPRIT schemes when Root Mean Square Error (RMSE) $> 0.3^{o}$. This accuracy is persuasive for most applications. Moreover, simulation results show the capability of the 3D-FOMP algorithm to detect adjacent signal sources and it outperforms the 3D-OMP, 3D-MUSIC and 3D-ESPRIT algorithms for all values of signal to noise ratio.

1. Introduction

Adaptive antennas and array processing have much important impacts to the performance of wireless communication networks. The problem of estimating angle of arrival signal is referred to Direction of Arrival (DOA) estimation problem. The DOA estimation is one of the most significant applications of adaptive antenna systems. It has a wide range of applications in different fields such as wireless communication systems [1,2], medical diagnosis and treatment, radar [3], sonar [4]. In DOA estimation applications, the main goal is to isolate arrival signals from different directions. An antenna array measures the received signals and employs signal processing algorithms to process the data and estimate directions. The information about DOAs can be useful for processing of multi-path components of the received signal or separation of a desired signal from interferences.

Numerous schemes have been proposed to obtain solutions for this problem. The beam scan schemes such as MVDR [5] and Root-MVDR [6] algorithms employ a conventional beam to scan a specific region to find DOAs according to the magnitude of the received signal. Subspace schemes use the signal and noise subspace orthogonality. The difficulty of these schemes is finding the signal and noise subspaces. Subspace based methods such as MUSIC [7], Root-MUSIC [8] and ESPRIT [9] have been developed and they have provided high performance which can approach the performance of a maximum likelihood algorithm. However, this performance is achieved at the expense of high computational cost. Moreover, high level of correlation in the received signals leads to serious performance degradation in these schemes. The maximum likelihood schemes are another class of DOA estimation schemes [10] which exploit statistical properties of the data, e.g., the covariance matrix. On the other hand, neural networks based [11] and support vector machine based [12] schemes work without the need of deriving the covariance matrix. They employ learning techniques to obtain

* Corresponding author.
E-mail address: aghababaiyan@ut.ac.ir (K. Aghababaiyan).

https://doi.org/10.1016/j.phycom.2018.10.005
1874-4907/

the statistical properties. However, they need a sufficiently large number of snapshots to derive the statistical properties.

Compressive sensing based algorithms are novel high resolution DOA estimation schemes which work according to the sparse property of the spatial spectrum [13]. They work efficiently even using one snapshot and this property is entirely different from other DOA estimation schemes. They provide efficient performance in high-dynamic scenarios where obtaining sufficient snapshots is hard. Several works in the literature such as [14,15] have discussed the advantages of these schemes. Compressive sensing schemes employ the convex relaxation algorithm [16,17] and the greedy algorithms [18–20]. The greedy algorithms are more computationally efficient; however, they suffer performance degradation.

The DOA estimation using compressive sensing schemes is a sparse representation problem over a redundant dictionary involving steering vectors of DOAs. The problem of selecting correct linear combination of these vectors is the same as the problem of selecting correct direction of arrival. The sparse representation problem is a Non-deterministic Polynomial-time hard (NP-hard) problem [18]. Greedy schemes such as Matching Pursuit (MP) [18], Orthogonal Matching Pursuit (OMP) [19] and Compressive Sampling Matching Pursuit (CSMP) [20] have been proposed in the literature for solving this problem.

Compressive sensing schemes improves resolution of DOA and reduces computational cost. The ML algorithm compares all feasible DOAs while compressive sensing schemes compare a small set of the angles to find DOAs in a smart method. Therefore, they are much more computationally efficient in comparison to the ESPRIT and MUSIC algorithms to converge to the ML solution. In addition, they approach to the ML solution even in low SNR scenarios, whereas other schemes converge at high SNR scenarios only. Moreover, in compressive sensing schemes the number of signal sources is not required to know and they can detect more signal sources than the antennas number while in other schemes the number of detectable DOAs is limited by the number of antennas. In spite of these advantages, compressive sensing schemes have a significant challenge owning to the coherence condition [21]. They cannot resolve two adjacent DOAs and they only find a single direction for the received composite signal. We have proposed Focused Orthogonal Matching Pursuit (FOMP) scheme in [22] for solving this challenge.

All compressive sensing based methods in the literature works for DOA estimation in two dimensional space. When we assume two dimensional space, the detection of signal sources which are out of the array plate is impossible. In practical applications, we need the DOA estimation in the three dimensional space, since the signal emitters are not always in the array plate. Hence, in this paper, we propose Three Dimensional Orthogonal Matching Pursuit (3D-OMP) algorithm for DOA estimation. In addition, we extend the FOMP scheme [22] to detect adjacent sources in three dimensional space. Therefore, the main contributions of this paper can be summarized as follows:

- We propose 3D-OMP algorithm for DOA estimation when we assume the signal sources and antenna array are located in three dimensional space. We provide a redundant dictionary for the 3D-OMP algorithm by employing azimuth and elevation angles.
- We investigate the capability of the proposed scheme to detect DOA of the signal sources via simulations in diverse scenarios for different values of SNR. Moreover, we analyze the efficiency of the 3D-OMP algorithm to detect multiple sources, simultaneously.
- We evaluate the accuracy of the estimated directions by the 3D-OMP algorithm via deriving the Cramer-Rao bound.

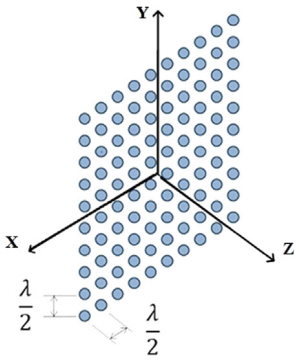

Fig. 1. A two dimensional $M \times M$ uniform linear array.

- We propose the extended version of FOMP scheme, i.e., 3D-FOMP scheme for DOA estimation to detect adjacent signal sources in three dimensional space.
- We investigate the efficiency of the 3D-FOMP algorithm for distinguishing between close signal emitters by simulation results.
- Finally, we compare the proposed DOA estimation schemes with existing methods in the literature in terms of the complexity and accuracy.

This paper is organized as follows. In Section 2, we present the system model. Then, we propose the 3D-OMP algorithm in Section 3. Next, we derive the Cramer-Rao bound of the 3D-OMP algorithm to evaluate its accuracy in Section 4. Then, we propose the 3D-FOMP scheme to distinguish between very close signal sources in Section 5. Next, we analyze the complexities of the proposed algorithms in Section 6. Simulation results are presented in Section 7 and Section 8 concludes the paper.

2. System model

In our system model, we consider a two-dimensional $M \times M$ elements uniform linear array. The distances between adjacent elements are $\frac{\lambda}{2}$ as shown in Fig. 1. We assume the signal to noise ratios are equivalent at the input of antenna elements. For describing the direction of signal emitters in three dimensional space, we employ the elevation angle, i.e., φ and the azimuth angle, i.e., θ. Fig. 2 shows these angles for an assumed signal emitter. Hence, one can express the base band received signals by antenna elements as

$$x(t) = \begin{pmatrix} s(t-\tau_{11})e^{jw_c\tau_{11}} & \dots & s(t-\tau_{1M})e^{jw_c\tau_{1M}} \\ \vdots & \ddots & \vdots \\ s(t-\tau_{M1})e^{jw_c\tau_{M1}} & \dots & s(t-\tau_{MM})e^{jw_c\tau_{MM}} \end{pmatrix}. \quad (1)$$

For a two dimensional linear array, we can express the propagation delay of the received signal by the element in row m and column n as

$$\tau_{mn} = \tau_0 - \frac{d_m^x}{c}\sin\theta\sin\varphi - \frac{d_n^y}{c}\sin\theta\cos\varphi, \quad (2)$$

where τ_0 is the propagation delay from the signal emitter to a reference point on the center of array, d_m^x is the distance between the elements in row m and the array reference point in the direction of axis X, d_n^y is the distance between the elements in column n and the array reference point in the direction of axis Y, c is the light velocity and φ, θ are the elevation and azimuth angles relative to the line perpendicular to the array. Without loss of generality, we consider $\tau_0 = 0$. Hence, we have

$$\tau_{mn} = -\frac{d_m^x}{c}\sin\theta\sin\varphi - \frac{d_n^y}{c}\sin\theta\cos\varphi. \quad (3)$$

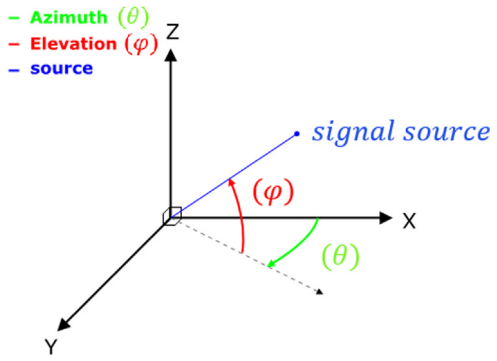

Fig. 2. The elevation angle, i.e., φ and the azimuth angle, i.e., θ for a signal emitter.

We consider D is the aperture of the antenna array in terms of the wavelength λ. When bandwidth of the signal is B and $B \ll \frac{f_c}{D}$, $s(t)$ can be considered to be narrow band. Therefore, we can consider $s(t-\tau_{mn}) \approx s(t)$. Thus, the received signals by the array elements can be expressed as

$$x(t) = s(t)\begin{pmatrix} e^{jw_c\tau_{11}} & \dots & e^{jw_c\tau_{1M}} \\ \vdots & \ddots & \vdots \\ e^{jw_c\tau_{M1}} & \dots & e^{jw_c\tau_{MM}} \end{pmatrix}. \tag{4}$$

We define $a(\theta, \varphi)$ as the array response to a unit amplitude signal, i.e., $s(t) = 1$.

$$a(\theta,\varphi) = \begin{pmatrix} a_{11}(\theta,\varphi) & \dots & a_{1M}(\theta,\varphi) \\ \vdots & \ddots & \vdots \\ a_{M1}(\theta,\varphi) & \cdots & a_{MM}(\theta,\varphi) \end{pmatrix}, \tag{5}$$

where

$$a_{mn}(\theta,\varphi) = \exp\left\{\frac{j2\pi}{\lambda}\sin\theta\left(d_m^x\sin\varphi + d_n^y\cos\varphi\right)\right\}. \tag{6}$$

In this paper, to achieve a comprehensive model to describe the received narrow band signal while considering the effect of noise and clutter, we express the received signal by antenna array when the signal emitter elevation and azimuth angles are φ_0 and θ_0, respectively as

$$y(t) = \sqrt{SNR}\,\beta\, s(t)a(\theta_0,\varphi_0) + v(t), \tag{7}$$

where $v(t)$ is a noise vector which contains independent zero-mean unit-variance Gaussian random variables and β shows the attenuation of the envelop of received signal due to the clutter effect. When radar illuminates a large patch of the ground, the probability distribution of the envelope of the received signal can be approximated by a Rayleigh distribution [23], since the signal can be considered as the sum of randomly phased components from a large number of independent scatters. Thus, we consider the probability distribution function of β as

$$f(\beta) = \frac{\beta}{\sigma^2}\exp(\frac{-\beta^2}{2\sigma^2}). \tag{8}$$

Moreover, in this model we consider the signal $s(t)$ has unit power.

3. 3D-OMP algorithm for DOA estimation

The OMP algorithm for DOA estimation can be described over $\mathbb{C}$ as follows. In this scheme, $Q = \{q_k\}_{k=1}^{K}$ is a highly redundant dictionary of vectors, i.e., $q_k \in \mathbb{C}^R$ and $R \ll K$ where $\mathbb{C}^R = \text{Span}(Q)$. This scheme is described as deriving a matrix A which is composed of the columns of dictionary Q, $A = [a_1, a_2, \dots, a_K]$ and $\bar{x}$ that satisfies

$$\|A\bar{x} - x\| \le \varepsilon, \tag{9}$$

with at most h non-zero entries such that $\varepsilon \ge 0$ and $h > 1$. The principal idea of the DOA estimation by the OMP algorithm is obtaining DOA via deriving the maximum correlation between the residual and the steering vectors of diverse DOAs which are not involved in the estimated DOA set. Moreover, the residual is re-computed by subtracting the contributions of the estimated DOAs. In this paper, we extend the OMP algorithm for DOA estimation in three dimensional space and propose the 3D-OMP algorithm.

In DOA estimation by the 3D-OMP algorithm, we employ the delay-and-sum beam forming processing [24]. The beam forming is implemented by using proper phase shifts. In the expression in (7), the received signal is described by the array manifold, i.e., $a(\theta, \varphi)$. In beam forming, the signals are combined in phase by using the complex conjugate of the array manifold. Assume

$$F(\theta,\varphi) = \left|a(\theta,\varphi)^H a(\theta_0,\varphi_0)\right|. \tag{10}$$

When the selected angles φ and θ are equivalent to the right emitter elevation and azimuth angles, we achieve the largest value of $F(\theta, \varphi)$ as

$$F(\theta_0,\varphi_0) = \left|a(\theta_0,\varphi_0)^H a(\theta_0,\varphi_0)\right| = M^2. \tag{11}$$

On the other hand, if $\theta \ne \theta_0$ or $\varphi \ne \varphi_0$, the signals are not added in phase, and thus, $F(\theta, \varphi)$ is smaller. Therefore, for the DOA estimation by the 3D-OMP algorithm, first $P(\theta, \varphi)$ is derived as

$$P(\theta,\varphi) = \left|W(\theta,\varphi)^H y\right|^2, \tag{12}$$

where

$$W(\theta,\varphi) = \frac{a(\theta,\varphi)}{|a(\theta,\varphi)|}. \tag{13}$$

Finally, peak-picking process is carried out by using the OMP algorithm to estimate DOA [14]. We describe the 3D-OMP algorithm in detail in the following.

- **Step 1:** First, consider dictionary $Q = \{P_n(\theta,\varphi|\theta_k,\varphi_k)\}_{\frac{-\pi}{2}\le\theta_k,\varphi_k\le\frac{\pi}{2}}$ where each element of this dictionary is defined as normalized $P(\theta,\varphi|\theta_k,\varphi_k)$ where $P(\theta,\varphi|\theta_k,\varphi_k)$ is obtained by the expression in (12) when y is the received signal from a signal source in θ_k and φ_k direction. Hence, $P_n(\theta,\varphi|\theta_k,\varphi_k)$, $k = 1, \dots, K$, have unit power.
$$P_n(\theta,\varphi|\theta_k,\varphi_k) = \frac{P(\theta,\varphi|\theta_k,\varphi_k)}{\sqrt{\frac{1}{K^2}\sum_{j=1}^{K}\sum_{j'=1}^{K}\left|P(\theta_j,\varphi_{j'}|\theta_k,\varphi_k)\right|^2}}. \tag{14}$$
- **Step 2:** The value of error in the first step of this algorithm is defined as
$$e_0(\theta,\varphi) = P(\theta,\varphi), \quad i = 1. \tag{15}$$
- **Step 3:** Then, we calculate the residuals for all angles of the dictionary as
$$e_i(\theta,\varphi|\theta_k,\varphi_k) = e_{i-1}(\theta,\varphi) - a_{i-1}(\theta_k,\varphi_k)P_n(\theta,\varphi|\theta_k,\varphi_k), \tag{16}$$
where $a_{i-1}(\theta_k,\varphi_k)$ is the inner product of $e_{i-1}(\theta,\varphi)$ and $P_n(\theta,\varphi|\theta_k,\varphi_k)$.
- **Step 4:** Next, according to values derived in Step 3, we select $\hat{\theta}_i$ and $\hat{\varphi}_i$ by minimizing the value of $|e_i(\theta,\varphi|\theta_k,\varphi_k)|^2$ as
$$\hat{\theta}_i, \hat{\varphi}_i = \arg\min_{\theta_k,\varphi_k}\left(|e_i(\theta,\varphi|\theta_k,\varphi_k)|^2\right). \tag{17}$$
- **Step 5:** If
$$\frac{\sum_{j=1}^{K}\sum_{j'=1}^{K}{e_0}^2(\theta_j,\varphi_{j'})}{\sum_{j=1}^{K}\sum_{j'=1}^{K}{e_i}^2(\theta_j,\varphi_{j'})} < \delta, \tag{18}$$

and also the number of iterations is smaller than the number of signal sources, i.e., S, return to step 3, or else end the algorithm. In (18), δ is the stopping criterion.

The estimated DOAs by the 3D-OMP algorithm are equivalent to the generalized likelihood estimated DOAs. Consider a general model for receiving signal as

$$y(t) = \gamma_0 a(\theta_0, \varphi_0) + v(t), \tag{19}$$

where $y(t)$ is the output signal vector, γ_0 is a complex scale factor, $a(\theta, \varphi)$ is the array manifold, θ_0 and φ_0 are the signal source azimuth and elevation angles, and $v(t)$ is the noise vector which contains independent Gaussian random variables with zero mean and unit-variance. The ML DOA estimation is obtained via joint minimization of the following error over θ_0, φ_0 and γ_0.

$$e(\theta_0, \varphi_0) = |y - \gamma_0 a(\theta_0, \varphi_0)|^2. \tag{20}$$

First, by minimizing over γ_0, we derive

$$\gamma_0 = \frac{a^H(\theta_0, \varphi_0) y}{a^H(\theta_0, \varphi_0) a(\theta_0, \varphi_0)}. \tag{21}$$

Then, by inserting γ_0 into (20), we have

$$e(\theta_0, \varphi_0) = \left| y - \frac{a^H(\theta_0, \varphi_0)\, y\, a(\theta_0, \varphi_0)}{a^H(\theta_0, \varphi_0)\, a(\theta_0, \varphi_0)} \right|^2. \tag{22}$$

Minimizing $e(\theta_0, \varphi_0)$ with respect to θ_0 and φ_0 is the same as maximizing

$$y^H \frac{a(\theta_0, \varphi_0) a^H(\theta_0, \varphi_0) y}{|a(\theta_0, \varphi_0)|^2}, \tag{23}$$

and the expression in (23) based on the expression in (13) is equivalent to $P(\theta_0, \varphi_0) = \left| W^H(\theta_0, \varphi_0) y \right|^2$. Therefore, the estimated DOA which is derived via beam forming analysis by maximizing $P(\theta, \varphi)$ is equivalent to the generalized likelihood estimated DOA.

4. Accuracy analysis of 3D-OMP algorithm using Cramer-Rao bound

Direction detection accuracy is measured by Mean Square Error (MSE) of the estimator. When we assume $\hat{\alpha}$ is the estimated direction and α is the true direction, for an unbiased estimator, we have $\mathbb{E}\{\hat{\alpha}\} = \alpha$. Therefore, MSE is equivalent to the variance of the estimated direction, i.e.,

$$\mathrm{MSE}\{\hat{\alpha}\} = \mathbb{E}\left\{ \left| \hat{\alpha} - \mathbb{E}\{\hat{\alpha}\} \right|^2 \right\} = \mathrm{VAR}\{\hat{\alpha}\}. \tag{24}$$

The Cramer-Rao Bound (CRB) is a useful tool for assessing the accuracy of DOA estimation schemes, as it provides a lower bound on the variance of any unbiased estimator. Assume z is a multivariate complex Gaussian vector with zero mean and covariance matrix R_z. Assume that R_z depends on a single unknown parameter α. Then the Fisher information matrix can be obtained as [25]

$$F = \mathrm{trace}\left\{ {R_z}^{-1} \frac{\delta R_z}{\delta \alpha} {R_z}^{-1} \frac{\delta R_z}{\delta \alpha} \right\}, \tag{25}$$

where

$$R_z = 2\sigma^2\, \mathrm{SNR}\, a(\theta, \varphi) a(\theta, \varphi)^H + I. \tag{26}$$

In the expression in (26), we have considered $E\{\beta^2\} = 2\sigma^2$. In the expression in (25), α can be one of θ or φ angles, and thus, we assume the other one is constant for deriving F. Then, the CRB of each angle is defined as $\mathrm{CRB} = \frac{1}{N} F^{-1}$ according to its Fisher value where N is the number of snapshots. To derive the CRB, we have

$$\frac{\delta R_z}{\delta \alpha} = 2\sigma^2\, \mathrm{SNR}\, \dot{a}(\theta, \varphi) a(\theta, \varphi)^H + 2\sigma^2\, \mathrm{SNR}\, a(\theta, \varphi) \dot{a}(\theta, \varphi)^H. \tag{27}$$

Therefore, we have

$$\begin{aligned} F = {} & 4\sigma^4\, \mathrm{SNR}^2 [\left(a(\theta, \varphi)^H {R_z}^{-1} \dot{a}(\theta, \varphi) \right)^2 \\ & + 2 \left(a(\theta, \varphi)^H {R_z}^{-1} a(\theta, \varphi) \right) \left(\dot{a}(\theta, \varphi)^H {R_z}^{-1} \dot{a}(\theta, \varphi) \right) \\ & + \left(\dot{a}(\theta, \varphi)^H {R_z}^{-1} a(\theta, \varphi) \right)^2]. \end{aligned} \tag{28}$$

Using the well-known matrix identity formula, i.e.,

$$(A + BCD)^{-1} = A^{-1} - A^{-1} B \left(C^{-1} + D A^{-1} B \right)^{-1} D A^{-1}, \tag{29}$$

and the expression in (26), we can derive

$${R_z}^{-1} = I - \frac{1}{1/(2\sigma^2\, \mathrm{SNR}) + a(\theta, \varphi)^H a(\theta, \varphi)} a(\theta, \varphi) a(\theta, \varphi)^H. \tag{30}$$

Thus, we have

$$\begin{aligned} a(\theta, \varphi)^H {R_z}^{-1} \dot{a}(\theta, \varphi)^H = {} & a(\theta, \varphi)^H \dot{a}(\theta, \varphi) \\ & - \frac{\left(a(\theta, \varphi)^H a(\theta, \varphi) \right) \left(a(\theta, \varphi)^H \dot{a}(\theta, \varphi) \right)}{1/(2\sigma^2\, \mathrm{SNR}) + a(\theta, \varphi)^H a(\theta, \varphi)}. \end{aligned} \tag{31}$$

Since $a(\theta, \varphi)^H \dot{a}(\theta, \varphi) = 0$, according to Appendix, the expression in (31) is zero. Similarly, the third term in (28) is zero as

$$\dot{a}(\theta, \varphi)^H {R_z}^{-1} a(\theta, \varphi) = \left(a(\theta, \varphi)^H {R_z}^{-1} \dot{a}(\theta, \varphi) \right)^H = 0. \tag{32}$$

We conclude that

$$F = 8\sigma^4\, \mathrm{SNR}^2 \left(a(\theta, \varphi)^H {R_z}^{-1} a(\theta, \varphi) \right) \left(\dot{a}(\theta, \varphi)^H {R_z}^{-1} \dot{a}(\theta, \varphi) \right). \tag{33}$$

Using the expression in (30), we obtain

$$\begin{aligned} a(\theta, \varphi)^H {R_z}^{-1} a(\theta, \varphi) &= |a(\theta, \varphi)|^2 - \frac{|a(\theta, \varphi)|^4}{1/(2\sigma^2\, \mathrm{SNR}) + |a(\theta, \varphi)|^2} \\ &= \frac{1}{2\sigma^2\, \mathrm{SNR}} \frac{|a(\theta, \varphi)|^2}{1/(2\sigma^2\, \mathrm{SNR}) + |a(\theta, \varphi)|^2}, \end{aligned} \tag{34}$$

and

$$\begin{aligned} \dot{a}(\theta, \varphi)^H {R_z}^{-1} \dot{a}(\theta, \varphi) = {} & \dot{a}(\theta, \varphi)^H \dot{a}(\theta, \varphi) \\ & - \frac{\left(\dot{a}(\theta, \varphi)^H a(\theta, \varphi) \right) \left(a(\theta, \varphi)^H \dot{a}(\theta, \varphi) \right)}{1/(2\sigma^2\, \mathrm{SNR}) + a(\theta, \varphi)^H a(\theta, \varphi)}. \end{aligned} \tag{35}$$

Since $\dot{a}(\theta, \varphi)^H a(\theta, \varphi) = 0$, the second term in (35) is zero. Thus, we can simplify the expression in (35) as

$$\dot{a}(\theta, \varphi)^H {R_z}^{-1} \dot{a}(\theta, \varphi) = |\dot{a}(\theta, \varphi)|^2. \tag{36}$$

Finally, by substituting the expressions in (34) and (36) into (33), we derive

$$F = 8\sigma^4\, \mathrm{SNR}^2 |\dot{a}(\theta, \varphi)|^2 \frac{|a(\theta, \varphi)|^2}{1/(2\sigma^2\, \mathrm{SNR}) + |a(\theta, \varphi)|^2}. \tag{37}$$

Note that we have $|a(\theta, \varphi)|^2 = M^2$, and therefore

$$\frac{|a(\theta, \varphi)|^2}{1/(2\sigma^2\, \mathrm{SNR}) + |a(\theta, \varphi)|^2} = \frac{2M^2\sigma^2\, \mathrm{SNR}}{2M^2\sigma^2\, \mathrm{SNR} + 1}. \tag{38}$$

When $2M^2\, \sigma^2\, \mathrm{SNR} >> 1$, we have $\frac{2M^2\sigma^2\, \mathrm{SNR}}{2M^2\sigma^2\, \mathrm{SNR}+1} \approx 1$, and hence, $F \approx 4\sigma^2\ \mathrm{SNR} |\dot{a}(\theta, \varphi)|^2$. Thus, the CRBs for $\hat{\theta}$ and $\hat{\varphi}$ are derived as, respectively

$$\mathrm{CRB}_\theta(\hat{\theta}) \approx \frac{1}{4N\, \sigma^2\, \mathrm{SNR} |\dot{a}(\theta, \varphi)|^2}, \tag{39}$$

$$\mathrm{CRB}_\varphi(\hat{\varphi}) \approx \frac{1}{4N\, \sigma^2\, \mathrm{SNR} \left| \dot{\tilde{a}}(\theta, \varphi) \right|^2}. \tag{40}$$

Thus, according to Appendix, the expressions in (39) and (40) are simplified as

$$\mathrm{CRB}_\theta(\hat{\theta}) \approx \frac{1}{4N\, \sigma^2\, \mathrm{SNR} \left(\frac{2\pi}{\lambda} \right)^2 \cos^2\theta \bar{d}^2}, \tag{41}$$

$$\mathrm{CRB}_{\varphi}(\hat{\varphi}) \approx \frac{1}{4N\,\sigma^2\,\mathrm{SNR}\left(\frac{2\pi}{\lambda}\right)^2 \sin^2\theta\,\bar{\bar{d}}^2}. \tag{42}$$

where

$$\bar{d}^2 = \frac{1}{M}\sum_{m=1}^{M}\left(d_m^x\right)^2\sin^2\varphi + \left(d_m^y\right)^2\cos^2\varphi + d_m^x d_m^y \sin 2\varphi, \tag{43}$$

and

$$\bar{\bar{d}}^2 = \frac{1}{M}\sum_{m=1}^{M}\left(d_m^x\right)^2\cos^2\varphi + \left(d_m^y\right)^2\sin^2\varphi - d_m^x d_m^y \sin 2\varphi. \tag{44}$$

5. Three dimensional focused orthogonal matching pursuit

Theoretical results show that the mutual coherence limits the success of the 3D-OMP algorithm. When two signal sources are adjacent, the situation becomes worse. Thus, the 3D-OMP algorithm cannot distinguish between them. Therefore, in this section, we propose 3D-FOMP scheme which can detect two adjacent signal emitters. In this scheme, the 3D-OMP algorithm is firstly used to obtain the initial estimated DOAs; then, 3D-FOMP algorithm is utilized to enhance DOAs estimation accuracy by minimizing the residuals. We propose the 3D-FOMP scheme by 9 steps in the following.

- **Step 1:** We consider dictionary $Q = \{P_n(\theta, \varphi|\theta_k, \varphi_k)\}_{\frac{-\pi}{2}\le\theta_k,\varphi_k\le\frac{\pi}{2}}$ where each element of this dictionary is defined as normalized $P(\theta, \varphi|\theta_k, \varphi_k)$ where $P(\theta, \varphi|\theta_k, \varphi_k)$ is obtained by the expression in (12) when y is the received signal from a signal source in θ_k and φ_k direction. Hence, $P_n(\theta, \varphi|\theta_k, \varphi_k)$, $k = 1, \ldots, K$, have unit power.

$$P_n(\theta, \varphi|\theta_k, \varphi_k) = \frac{P(\theta, \varphi|\theta_k, \varphi_k)}{\sqrt{\frac{1}{K^2}\sum_{j=1}^{K}\sum_{j'=1}^{K}\left|P(\theta_j, \varphi_{j'}|\theta_k, \varphi_k)\right|^2}}. \tag{45}$$

- **Step 2:** The value of error in the first step of this algorithm is defined as

$$e_0(\theta, \varphi) = P(\theta, \varphi), \quad i = 1. \tag{46}$$

- **Step 3:** Then, we calculate the residuals for all angles of the dictionary as

$$e_i(\theta, \varphi|\theta_k, \varphi_k) = e_{i-1}(\theta, \varphi) - a_{i-1}(\theta_k, \varphi_k)P_n(\theta, \varphi|\theta_k, \varphi_k), \tag{47}$$

where $a_{i-1}(\theta_k, \varphi_k)$ is the inner product of $e_{i-1}(\theta, \varphi)$ and $P_n(\theta, \varphi|\theta_k, \varphi_k)$.

- **Step 4:** Next, according to the derived values in Step 3, we select $\hat{\theta}_i$ and $\hat{\varphi}_i$ by minimizing the value of $|e_i(\theta, \varphi|\theta_k, \varphi_k)|^2$ as

$$\hat{\theta}_i, \hat{\varphi}_i = \underset{\theta_k,\varphi_k}{\arg\min}\left(|e_i(\theta, \varphi|\theta_k, \varphi_k)|^2\right). \tag{48}$$

We save $\hat{\theta}_i$ and $\hat{\varphi}_i$ in the system memory. When there is a pair of adjacent sources, 3D-OMP algorithm only finds a direction between the right directions. Thus, we assume there is a pair of sources in the adjacency of $\hat{\theta}_i$ and $\hat{\varphi}_i$ angles.

- **Step 5:** Next, we derive the residuals for all pair of $(\theta_{k1}, \varphi_{k1})$ and $(\theta_{k2}, \varphi_{k2})$ as

$$\begin{aligned} e_i'(\theta, \varphi|\theta_{k1}, \varphi_{k1}, \theta_{k2}, \varphi_{k2}) &= e_{i-1}(\theta, \varphi) \\ &- a_{i-1}(\theta_{k1}, \varphi_{k1})P_n(\theta, \varphi|\theta_{k1}, \varphi_{k1}) \\ &- a_{i-1}(\theta_{k2}, \varphi_{k2})P_n(\theta, \varphi|\theta_{k2}, \varphi_{k2}), \end{aligned} \tag{49}$$

where $(\theta_{k1}, \varphi_{k1})$ and $(\theta_{k2}, \varphi_{k2})$ are defined in $\hat{\theta}_i - \frac{BW_\theta}{2} \le \theta_{k1}, \theta_{k2} \le \hat{\theta}_i + \frac{BW_\theta}{2}$ and $\hat{\varphi}_i - \frac{BW_\varphi}{2} \le \varphi_{k1}, \varphi_{k2} \le \hat{\varphi}_i + \frac{BW_\varphi}{2}$ intervals that BW_θ is the beam width in the azimuth angle direction and BW_φ is the beam width in the elevation angle direction.

- **Step 6:** Next, according to the derived values in Step 5, we select $\hat{\theta}_{i1}, \hat{\varphi}_{i1}$ and $\hat{\theta}_{i2}, \hat{\varphi}_{i2}$ by minimizing the value of $\left|e_i'(\theta, \varphi|\theta_{k1}, \varphi_{k1}, \theta_{k2}, \varphi_{k2})\right|^2$ as

$$\begin{aligned} &\left(\hat{\theta}_{i1}, \hat{\varphi}_{i1}, \hat{\theta}_{i2}, \hat{\varphi}_{i2}\right) \\ &= \underset{\theta_{k1},\varphi_{i1},\theta_{k2},\varphi_{i2}}{\arg\min}\left(\left|e_i'(\theta, \varphi|\theta_{k1}, \varphi_{k1}, \theta_{k2}, \varphi_{k2})\right|^2\right). \end{aligned} \tag{50}$$

- **Step 7:** If $e_i'(\theta, \varphi|\hat{\theta}_{i1}, \hat{\varphi}_{i1}, \hat{\theta}_{i2}, \hat{\varphi}_{i2}) \le e_i(\theta, \varphi|\hat{\theta}_i, \hat{\varphi}_i)$, we can conclude our assumption is correct and there are a pair of sources in the adjacency of the angles $\hat{\theta}_i$ and $\hat{\varphi}_i$. Thus, we have $\hat{\theta}_i = \hat{\theta}_{i1}, \hat{\theta}_{i+1} = \hat{\theta}_{i2}, \hat{\varphi}_i = \hat{\varphi}_{i1}, \hat{\varphi}_{i+1} = \hat{\varphi}_{i2}, i = i + 2$. Therefore, the residual according to the detected sources is obtained as

$$\begin{aligned} e_i(\theta, \varphi) &= e_{i-2}(\theta, \varphi) - a_{i-2}(\hat{\theta}_{i1}, \hat{\varphi}_{i1})P_n(\theta, \varphi|\hat{\theta}_{i1}, \hat{\varphi}_{i1}) \\ &- a_{i-2}(\hat{\theta}_{i2}, \hat{\varphi}_{i2})P_n(\theta, \varphi|\hat{\theta}_{i2}, \hat{\varphi}_{i2}). \end{aligned} \tag{51}$$

- **Step 8:** If $e_i'(\theta, \varphi|\hat{\theta}_{i1}, \hat{\varphi}_{i1}, \hat{\theta}_{i2}, \hat{\varphi}_{i2}) > e_i(\theta, \varphi|\hat{\theta}_i, \hat{\varphi}_i)$, we can conclude the detected direction by the 3D-OMP algorithm is correct and there is only one source in the adjacency of the angles $\hat{\theta}_i$ and $\hat{\varphi}_i$. Thus, we have $\hat{\theta}_i = \hat{\theta}_i, \hat{\varphi}_i = \hat{\varphi}_i, i = i + 1$. Therefore, the residual according to the detected source is obtained as

$$e_i(\theta, \varphi) = e_{i-1}(\theta, \varphi) - a_{i-1}(\hat{\theta}_i, \hat{\varphi}_i)P_n(\theta, \varphi|\hat{\theta}_i, \hat{\varphi}_i). \tag{52}$$

- **Step 9:** If

$$\frac{\sum_{j=1}^{K}\sum_{j'=1}^{K} e_0{}^2(\theta_j, \varphi_{j'})}{\sum_{j=1}^{K}\sum_{j'=1}^{K} e_i{}^2(\theta_j, \varphi_{j'})} < \delta, \tag{53}$$

and also the number of iterations is smaller than the number of sources, i.e., S, return to Step 3, or else end the algorithm. In the expression in (53), δ is the stopping criterion.

6. Complexity analysis of 3D-OMP and 3D-FOMP algorithms

In this section, we compare the complexities of our proposed algorithms for DOA estimation with some former schemes. We assume that the number of antenna elements is $M \times M$, the number of signal sources is S, the number of exploited snapshots is N and the size of dictionary is $K \times K$ where K is the number of assumed azimuth and elevation angles.

In the 3D-OMP algorithm, we should calculate $P(\theta, \varphi)$ before starting the iterative algorithm. To derive $P(\theta, \varphi)$ according to the expression in (12), we need $M^2 N$ operations to calculate the product of $W(\theta, \varphi)$ and y for every θ and φ. Thus, the order of operations to derive $P(\theta, \varphi)$ is $O(K^2 M^2 N)$. Then, we analyze the number of required operations for implementation of different steps of the 3D-OMP algorithm. In Step 1, to normalize the dictionary elements, the order of required operations is $O(K^2)$. Furthermore, in Step 3 to calculate the residuals, the order of required operations is $O(K^2)$ and we need $O(K^2)$ operations to minimize $|e_i(\theta, \varphi|\theta_k, \varphi_k)|^2$ in Step 4. The complexity of Step 5 is in order of $O(K^2)$ to calculate the summations. The operations of Step 2 is negligible, since it only use $P(\theta, \varphi)$ that we derived before the beginning of the iterative algorithm. Therefore, the required operations for each iteration of this algorithm is in order of $O(K^2)$. Since we repeat the iterative part of the 3D-OMP algorithm to find all of signal sources, the complexity order of iterative part of the 3D-OMP is $O(K^2 S)$. Hence, the total complexity of the 3D-OMP algorithm is in order of $O(K^2 M^2 N) + O(K^2 S)$.

Similarly, in the 3D-FOMP algorithm, we should calculate $P(\theta, \varphi)$ before starting the iterative algorithm where the order of operations to derive $P(\theta, \varphi)$ is $O(K^2 M^2 N)$. Then, we study the number of required operations for implementation of different steps of the 3D-FOMP algorithm. Step 1 to 4 of the 3D-FOMP

Table 1
Complexity order of different schemes.

Scheme	Complexity order
3D-MUSIC	$O(M^4 P + M^4 N)$ [28]
3D-ESPRIT	$O(M^6 + M^4 N)$ [28]
3D-OMP	$O(K^2 M^2 N) + O(K^2 S)$
3D-FOMP	$O(K^2 M^2 N) + \max(O(K^2 S), O(K'^4 S))$

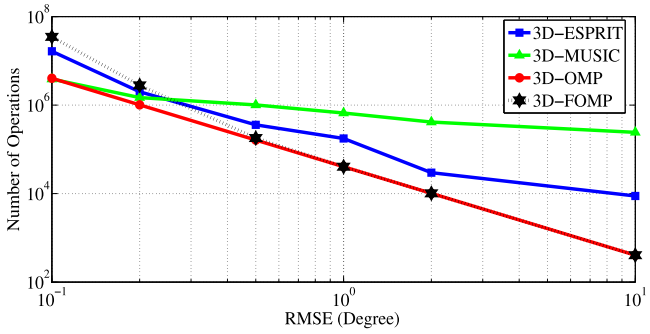

Fig. 3. Number of operations of different schemes to provide different values of RMSE.

algorithm are similar to the 3D-OMP algorithm. In Step 5, the number of pairs of angles is $\binom{K'}{2} = \frac{K'(K'-1)}{2}$ where K' is the number of angles in azimuth and evolution beamwidth. Thus, the order of complexity of this step is $O(K'^4)$. Moreover, we need $O(K'^4)$ operations to minimize $\left|e_i'(\theta, \varphi|\theta_{k1}, \varphi_{k1}, \theta_{k2}, \varphi_{k2})\right|^2$ at Step 6. The complexities of Steps 7 and 8 are in order of $O(K^2)$ to calculate the residuals. Finally, the complexity of Step 9 is in order of $O(K^2)$ to calculate the summations. Since we repeat the iterative part of the 3D-FOMP algorithm to find all signal sources, the complexity order of iterative part of the 3D-FOMP is $\max(O(K^2 S), O(K'^4 S))$. Hence, the total complexity of the 3D-FOMP algorithm is in order of $O(K^2 M^2 N) + \max(O(K^2 S), O(K'^4 S))$. Usually, the number of angles in beamwidth of the array antenna is smaller than the total number of angles and we can consider $K' \ll K$. According to this assumption, we conclude that the complexities of the 3D-OMP and 3D-FOMP algorithms are in the same order. Table 1 lists the order of complexities of different three dimensional DOA estimation schemes. In addition, Fig. 3 shows the number of operations of different schemes to achieve different amount of accuracy. It can be seen, the 3D-OMP algorithm has a lower complexity in comparison to the 3D-MUSIC [26] and 3D-ESPRIT [27] schemes for different values of Root Mean Square Error (RMSE). However, the 3D-FOMP algorithm has a lower complexity in comparison to the 3D-MUSIC and 3D-ESPRIT schemes when RMSE $>$ 0.3^o. This accuracy is persuasive for most applications.

To investigate the impact of Doppler effect, we assume the signal source moves with velocity V in our scenario. In this situation, Doppler frequency is obtained as

$$f_0 = \frac{f_c}{c} V, \tag{54}$$

where f_c is the frequency of the signal source. Thus, by considering the Doppler effect, the received signal can be written as

$$y(t) = \sqrt{SNR}\beta s(t) e^{-j2\pi f_0} a(\theta_0, \varphi_0) + v(t). \tag{55}$$

By replacing the expression in (55) into (12), we have

$$P(\theta, \varphi) = \left|W(\theta, \varphi)^H (\sqrt{SNR}\beta s(t) e^{-j2\pi f_0} a(\theta_0, \varphi_0) + v(t))\right|^2. \tag{56}$$

When the value of SNR is high, the second term is negligible, and thus, the term $e^{-j2\pi f_0}$ is effectless for DOA estimation by the 3D-OMP and 3D-FOMP algorithms, since $\left|e^{-j2\pi f_0}\right| = 1$.

Table 2
Simulation parameters.

Parameter	Description
Frequency of signal source (f_c)	1 GHz
Number of antenna ($M \times M$)	10×10
Number of snapshots (N)	1
Stopping criterion (δ)	0.01
SNR values	-10 to 20 (dB)
Clutter effect (σ)	0.5
Number of runs	1000
Number of θ and φ (K)	180
Distribution of selected θ and φ	Random

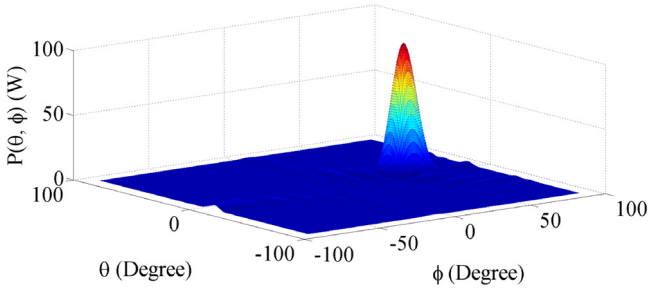

Fig. 4. $P(\theta, \varphi)$ for a 10×10 array when there is a signal source in $\theta_0 = \frac{\pi}{18}, \varphi_0 = \frac{5\pi}{18}$ direction and SNR $= 20$ dB.

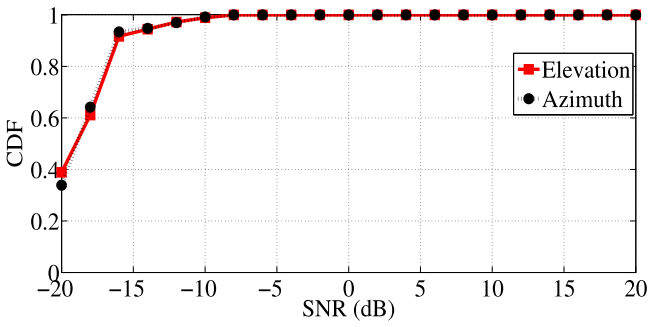

Fig. 5. Cumulative distribution function of the probability of correct detections for the elevation and azimuth angles when the 3D-OMP algorithm is employed for DOA estimation versus different SNRs.

7. Simulation results

In this section, we evaluate the performance of the 3D-OMP algorithm for diverse values of SNRs. First, we assume a scenario where there is only one signal emitter. We tabulate the simulation parameters in Table 2. We repeat our simulations 1000 times for different directions and report the average results. Fig. 4 shows $P(\theta, \varphi)$ when there is a single source in $\theta_0 = \frac{\pi}{18}$, $\varphi_0 = \frac{5\pi}{18}$ direction for SNR $= 20$ dB. Moreover, Fig. 5 shows the Cumulative Distribution Function (CDF) of the probability of correct detections in the 3D-OMP algorithm for different values of signal to noise ratios. As can be observed, the 3D-OMP algorithm has a high performance for SNRs higher than -10 dB and it provides an unbiased estimation for azimuth and elevation angles. Moreover, Fig. 6 shows the variances of the estimated angles. It can be seen that the variances are close to the CRBs.

Next, we analyze the efficiency of the 3D-OMP algorithm to detect multiple sources, simultaneously. We assume a scenario where two signals are received by the array antenna from (θ_1, φ_1) and (θ_2, φ_2) directions. Therefore, the received signal can be expressed as

$$y(t) = \sqrt{\text{SNR}_1}\,\beta_1 S_1(t) a(\theta_1, \varphi_1)$$

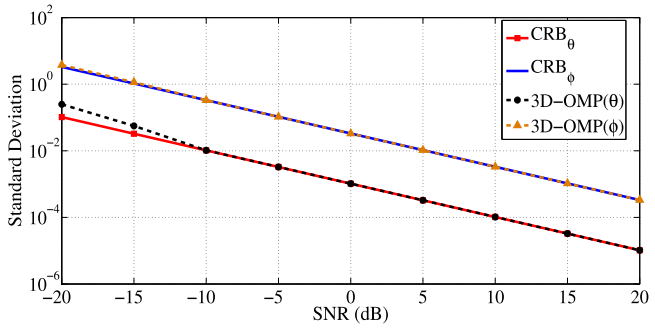

Fig. 6. The standard deviation of the estimated angles by the 3D-OMP algorithm and their CRBs.

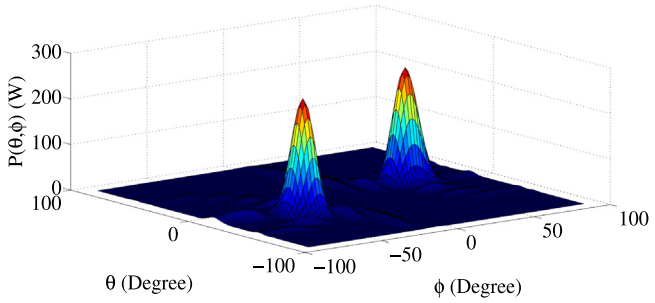

Fig. 7. $P(\theta, \varphi)$ for a 10×10 array when there are two signal sources in $\theta_1 = \frac{\pi}{18}$, $\varphi_1 = \frac{5\pi}{18}$ and $\theta_2 = \frac{-\pi}{9}$, $\varphi_2 = \frac{-2\pi}{9}$ directions and SNR $= 20$ dB.

$$+ \sqrt{\text{SNR}_2}\, \beta_2\, S_2(t) a(\theta_2, \varphi_2) + v(t), \tag{57}$$

where SNR_1 and SNR_2 are the signal to noise ratios of the signal sources which are located in (θ_1, φ_1) and (θ_2, φ_2) directions, respectively. Moreover, β_1 and β_2 show the attenuation of the envelop of their signals due to the clutter effect. The expected value of $P(\theta, \varphi)$ can be derived as

$$\begin{aligned} E\{P(\theta,\varphi)\} &= \text{SNR}_1 E\{{\beta_1}^2\} \left| W(\theta,\varphi)^H a(\theta_1,\varphi_1) \right|^2 \\ &\quad + \text{SNR}_2 E\{{\beta_2}^2\} \left| W(\theta,\varphi)^H a(\theta_2,\varphi_2) \right|^2 \\ &\quad + 2\rho_{12} E\{\beta_1\beta_2\} \sqrt{\text{SNR}_1}\sqrt{\text{SNR}_2}\, \text{Re}\{W(\theta,\varphi)^H \\ &\quad \times a(\theta_1,\varphi_1)(W(\theta,\varphi) a(\theta_2,\varphi_2))^*\} + 1, \end{aligned} \tag{58}$$

where $\rho_{12} = E\{s_1 {s_2}^*\}$, $E\left\{|s_1|^2\right\} = E\left\{|s_2|^2\right\} = 1$ and $Re\{.\}$ denotes the real part. Two signals can be assumed uncorrelated when they originate from two different signal sources. Thus, since $\rho_{12} = 0$, we can simplify the expression in (58) as

$$\begin{aligned} E\{P(\theta,\varphi)\} &= 2\sigma^2\, \text{SNR}_1 \left| W(\theta,\varphi)^H a(\theta_1,\varphi_1) \right|^2 \\ &\quad + 2\sigma^2\, \text{SNR}_2 \left| W(\theta,\varphi)^H a(\theta_2,\varphi_2) \right|^2 + 1. \end{aligned} \tag{59}$$

In the expression in (59), we have considered $E\{{\beta_1}^2\} = E\{{\beta_2}^2\} = 2\sigma^2$. We assume a scenario where there are two signal sources in $\theta_1 = \frac{\pi}{18}$, $\varphi_1 = \frac{5\pi}{18}$ and $\theta_2 = \frac{-\pi}{9}$, $\varphi_2 = \frac{-2\pi}{9}$ directions. Other parameters of this scenario are selected according to Table 2. Fig. 7 shows $P(\theta, \varphi)$ in this scenario when SNR $= 20$ dB. Fig. 8 shows the real locations and the estimated locations of the detected signal sources in this scenario by the 3D-OMP algorithm. In this figure, bigger circles and smaller circles show the real and estimated locations of signal sources, respectively. As can be observed, the direction of arrival of signal emitters are estimated exactly.

Then, we consider a scenario where there are a pair of close signal sources. In this scenario, we assume SNR $=$ 10 dB in the input of all antenna elements. Moreover, we consider signal sources are located in $\theta_1 = 10^o$, $\varphi_1 = 10^o$ and $\theta_2 = 17.5^o$, $\varphi_2 = 17.5^o$ directions. Fig. 9 shows $P(\theta, \varphi)$ which has a single peak corresponding to a direction between (θ_1, φ_1) and (θ_2, φ_2). Thus, the 3D-OMP algorithm cannot detect directions of signal sources in this scenario and we should employ the 3D-FOMP algorithm to detect signal sources.

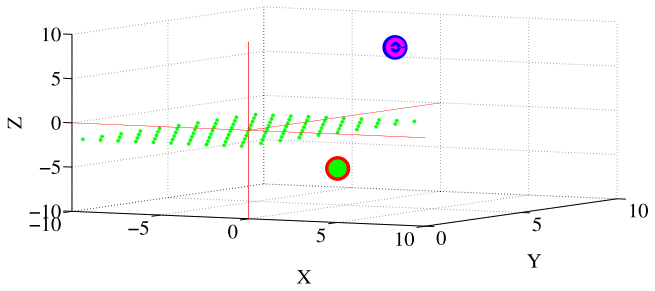

Fig. 8. The locations of the detected sources when we consider two signal sources in $\theta_1 = \frac{\pi}{18}$, $\varphi_1 = \frac{5\pi}{18}$ and $\theta_2 = \frac{-\pi}{9}$, $\varphi_2 = \frac{-2\pi}{9}$ directions.

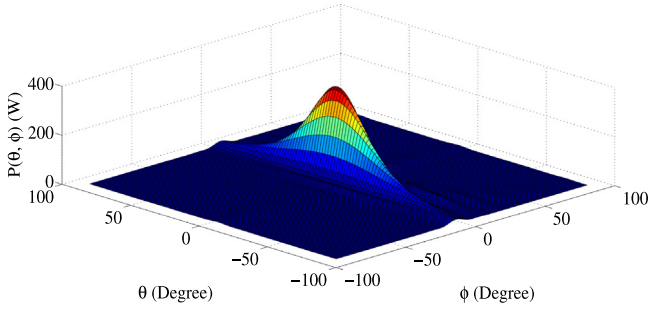

Fig. 9. $P(\theta, \varphi)$ when there are two pairs of adjacent signal sources in $\theta_1 = 10^o$, $\varphi_1 = 10^o$ and $\theta_2 = 17.5^o$, $\varphi_2 = 17.5^o$ directions.

Figs. 10 and 11 compare the 3D-OMP and 3D-FOMP algorithms with the 3D-MUSIC and 3D-ESPRIT algorithms in terms of RMSE of the azimuth and elevation angles for different values of SNR when we consider two signal sources and their distance exceeds the antenna beamwidth. As can be seen, the 3D-OMP and 3D-FOMP algorithms provide the same performance and they outperform the 3D-MUSIC and 3D-ESPRIT algorithms. By enhancing SNR, the 3D-MUSIC and 3D-ESPRIT approach to them in terms of RMSE.

Figs. 12 and 13 compare the 3D-OMP and 3D-FOMP algorithms with the 3D-MUSIC and 3D-ESPRIT algorithms in terms of RMSE of the azimuth and elevation angles for different values of SNR when we consider two adjacent sources in three dimensional space. We use the parameters of Table 2 for our simulations. As can be observed, the 3D-FOMP algorithm outperforms the 3D-OMP, 3D-MUSIC and 3D-ESPRIT algorithms. By enhancing SNR, the 3D-MUSIC and 3D-ESPRIT approach to the 3D-FOMP method in terms of RMSE of azimuth and elevation angles. However, the 3D-FOMP algorithm has a higher performance in comparison to the 3D-OMP algorithm for all values of SNR.

8. Conclusion

In this paper, we extended the OMP algorithm and have proposed the 3D-OMP algorithm for DOA estimation in three dimensional space. Simulation results have shown the high performance of the 3D-OMP algorithm for the SNR values higher than -10 dB. Moreover, results have shown that 3D-OMP algorithm can detect multiple sources, simultaneously. In addition, we have verified the accuracy of the estimated directions by 3D-OMP algorithm and we have seen the variances of the estimated angles are close to the CRBs. Since 3D-OMP algorithm cannot distinguish between

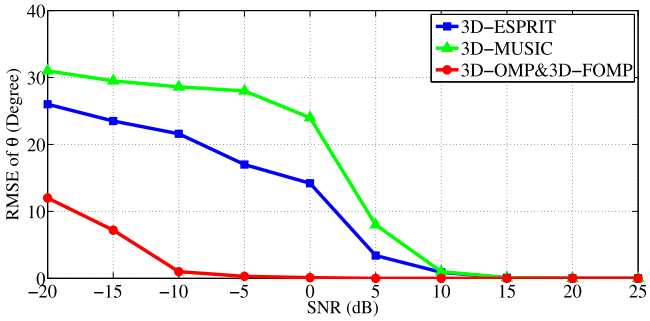

Fig. 10. The RMSE of azimuth angle for the 3D-OMP, 3D-FOMP, 3D-MUSIC and 3D-ESPRIT algorithms versus different values of SNR when we assume two signal sources in our scenario and their distance exceeds the beamwidth.

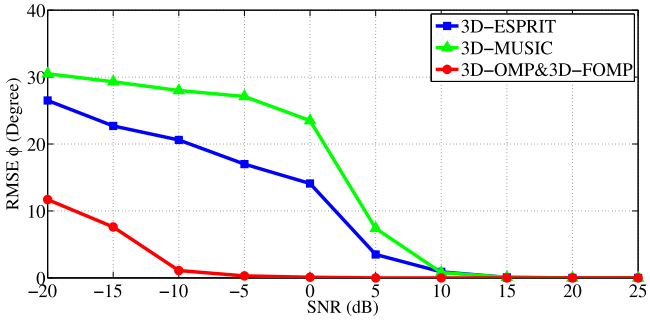

Fig. 11. The RMSE of elevation angle for the 3D-OMP, 3D-FOMP, 3D-MUSIC and 3D-ESPRIT algorithms versus different values of SNR when we assume two signal sources in our scenario and their distance exceeds the beamwidth.

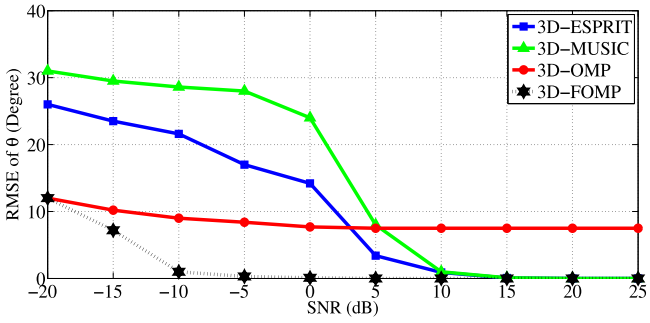

Fig. 12. The RMSE of azimuth angle for the 3D-OMP, 3D-FOMP, 3D-MUSIC and 3D-ESPRIT algorithms versus different values of SNR when we assume two adjacent signal sources in our scenario.

two adjacent signal sources, we have proposed the 3D-FOMP algorithm. We have seen 3D-OMP and 3D-FOMP algorithms have lower complexities in compression to 3D-MUSIC and 3D-ESPRIT schemes when RMSE $> 0.3^o$. In addition, simulation results have shown the 3D-FOMP algorithm have outperformed the 3D-OMP, 3D-MUSIC and 3D-ESPRIT algorithms for all values of SNR.

Appendix. Norm of first derivatives of array manifold

For the array manifold which is described in (5), the first derivatives in respect to θ and φ are derived as

$$\dot{a}(\theta,\varphi) = \frac{d}{d\theta}a(\theta,\varphi) = j\frac{2\pi}{\lambda}\cos\theta D a(\theta,\varphi), \tag{A.1}$$

$$\dot{\tilde{a}}(\theta,\varphi) = \frac{d}{d\varphi}a(\theta,\varphi) = j\frac{2\pi}{\lambda}\sin\theta \tilde{D} a(\theta,\varphi). \tag{A.2}$$

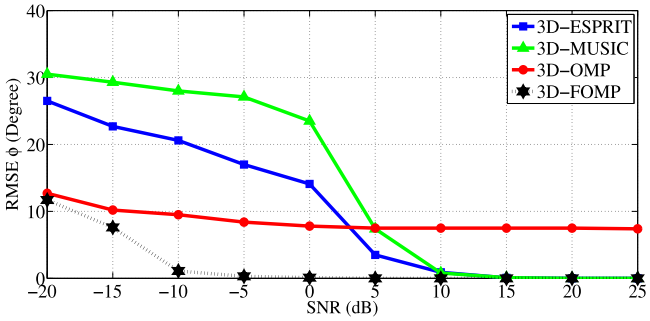

Fig. 13. The RMSE of elevation angle for the 3D-OMP, 3D-FOMP, 3D-MUSIC and 3D-ESPRIT algorithms versus different values of SNR when we assume two adjacent signal sources in our scenario.

In the expressions in (A.1) and (A.2), D and $\tilde{D}$ are defined as

$$D = \mathrm{diag}\left\{(d_1, d_2, \ldots, d_M)\right\}, \tag{A.3}$$

$$\tilde{D} = \mathrm{diag}\left\{\left(\tilde{d}_1, \tilde{d}_2, \ldots, \tilde{d}_M\right)\right\}, \tag{A.4}$$

where $d_i = d_i^x \sin\varphi + d_i^y \cos\varphi$ and $\tilde{d}_i = d_i^x \cos\varphi - d_i^y \sin\varphi$. Thus, we can derive

$$a(\theta,\varphi)^H \dot{a}(\theta,\varphi) = j\frac{2\pi}{\lambda}\cos\theta \sum_{m=1}^{M} d_m, \tag{A.5}$$

$$a(\theta,\varphi)^H \dot{\tilde{a}}(\theta,\varphi) = j\frac{2\pi}{\lambda}\sin\theta \sum_{m=1}^{M} \tilde{d}_m. \tag{A.6}$$

Without loss of generality the distances d_m and $\tilde{d}_m$ can be defined relative to the phase center of the array that $\sum_{m=1}^{M} d_m = 0$ and $\sum_{m=1}^{M} \tilde{d}_m = 0$. Hence, we can assume

$$a(\theta,\varphi)^H \dot{a}(\theta,\varphi) = 0, \tag{A.7}$$

$$a(\theta,\varphi)^H \dot{\tilde{a}}(\theta,\varphi) = 0. \tag{A.8}$$

Moreover, the norms of $\dot{a}(\theta,\varphi)$ and $\dot{\tilde{a}}(\theta,\varphi)$ are obtained as

$$|\dot{a}(\theta,\varphi)|^2 = \dot{a}(\theta,\varphi)^H \dot{a}(\theta,\varphi) = \left(\frac{2\pi}{\lambda}\right)^2 \cos^2\theta \bar{d}^2, \tag{A.9}$$

$$\left|\dot{\tilde{a}}(\theta,\varphi)\right|^2 = \dot{\tilde{a}}(\theta,\varphi)^H \dot{\tilde{a}}(\theta,\varphi) = \left(\frac{2\pi}{\lambda}\right)^2 \sin^2\theta \bar{\tilde{d}}^2. \tag{A.10}$$

References

[1] K. Aghababaiyan, B. Maham, QoS-aware downlink radio resource management in OFDMA-based small cells networks, IET Commun. 12 (4) (2018) 441–448, http://dx.doi.org/10.1049/iet-com.2017.1222.

[2] K. Aghababaiyan, B. Maham, Downlink radio resource allocation in OFDMA-based small cells networks, in: IEEE Black Sea Conference on Communications and Networking, BlackSeaCom, 2017, pp. 1–5. http://dx.doi.org/10.1109/BlackSeaCom.2017.8277707.

[3] A. Khabbazibasmenj, A. Hassanien, S.A. Vorobyov, M.W. Morency, Efficient transmit beamspace design for search-free based DOA estimation in MIMO radar, IEEE Trans. Signal Process. 62 (6) (2014) 1490–1500.

[4] W. Shi, J. Huang, Y. Hou, Fast DOA estimation algorithm for MIMO sonar based on ant colony optimization, J. Syst. Eng. Electron. 23 (2) (2012) 173–178.

[5] S.W. Varade, K.D. Kulat, Robust algorithms for DOA estimation and adaptive beamforming for smart antenna application, in: 2nd International Conference on Emerging Trends in Engineering and Technology, ICETET, 2009, pp. 1195–1200, http://dx.doi.org/10.1109/ICETET.2009.194.

[6] S.-W. Chen, C.-L. Meng, A.-C. Chang, DOA and DOD estimation based on double 1-D Root-MVDR estimators for bistatic MIMO radars, Wirel. Pers. Commun. 86 (3) (2016) 1321–1332.

[7] R. Schmidt, Multiple emitter location and signal parameter estimation, IEEE Trans. Antennas and Propagation 34 (3) (1986) 276–280.

[8] B. Friedlander, The Root- MUSIC algorithm for direction finding with interpolated arrays, Signal Process. 30 (1) (1993) 15–29.
[9] R. Roy, T. Kailath, ESPRIT-estimation of signal parameters via rotational invariance techniques, IEEE Trans. Acoust. Speech Signal Process. 37 (7) (1989) 984–995.
[10] P. Stoica, A. Nehorai, MUSIC, maximum likelihood, and Cramer- Rao bound: further results and comparisons, IEEE Trans. Acoust. Speech Signal Process. 38 (12) (1990) 2140–2150.
[11] M. Donelli, F. Viani, P. Rocca, A. Massa, An innovative multiresolution approach for DOA estimation based on a support vector classification, IEEE Trans. Antennas and Propagation 57 (8) (2009) 2279–2292.
[12] A.H. El Zooghby, C.G. Christodoulou, M. Georgiopoulos, A neural network-based smart antenna for multiple source tracking, IEEE Trans. Antennas and Propagation 48 (5) (2000) 768–776.
[13] D. Malioutov, M. Cetin, A.S. Willsky, A sparse signal reconstruction perspective for source localization with sensor arrays, IEEE Trans. Signal Process. 53 (8) (2005) 3010–3022.
[14] M. Carlin, P. Rocca, G. Oliveri, F. Viani, A. Massa, Directions of arrival estimation through bayesian compressive sensing strategies, IEEE Trans. Antennas and Propagation 61 (7) (2013) 3828–3838.
[15] G.Z. Karabulut, T. Kurt, A. Yongaçoglu, Estimation of directions of arrival by matching pursuit (EDAMP), EURASIP J. Wirel. Commun. Netw. 2005 (2) (2005) 197–205.
[16] E.J. Candès, J. Romberg, T. Tao, Robust uncertainty principles: Exact signal reconstruction from highly incomplete frequency information, IEEE Trans. Inform. Theory 52 (2) (2006) 489–509.
[17] S.S. Chen, D.L. Donoho, M.A. Saunders, Atomic decomposition by basis pursuit, SIAM Rev. 43 (1) (2001) 129–159.
[18] S.G. Mallat, Z. Zhang, Matching pursuits with time-frequency dictionaries, IEEE Trans. Signal Process. 41 (12) (1993) 3397–3415.
[19] J.A. Tropp, A.C. Gilbert, Signal recovery from random measurements via orthogonal matching pursuit, IEEE Trans. Inform. Theory 53 (12) (2007) 4655–4666.
[20] D. Needell, J.A. Tropp, CoSaMP: iterative signal recovery from incomplete and inaccurate samples, Commun. ACM 53 (12) (2010) 93–100.
[21] A.M. Kondoz, Digital Speech: Coding for Low Bit Rate Communication Systems, John Wiley & Sons, 2005.
[22] M. Dehghani, K. Aghababaiyan, FOMP algorithm for direction of arrival estimation, Phys. Commun. 26 (2018) 170–174.
[23] H. Goldstein, D.E. Kerr, Propagation of short radio waves, Mass. Inst. Tech. Radiation Lab, 1951, pp. 588–640.
[24] M. Karaman, P.C. Li, M. O'Donnell, Synthetic aperture imaging for small scale systems, IEEE Trans. Ultrason. Ferroelectr. Freq. Control 42 (3) (1995) 429–442.
[25] J.A. Hoeting, D. Madigan, A.E. Raftery, C.T. Volinsky, Bayesian model averaging: a tutorial, Stat. Sci. (1999) 382–401.
[26] Z. Ping, S. Haoshan, S. Kui, The 3D location algorithm based on Smart antenna with MUSIC DOA estimates, in: World Congress on Computer Science and Information Engineering, vol. 4, March 2009, pp. 750–753, http://dx.doi.org/10.1109/CSIE.2009.123.
[27] P. Strobach, Total least squares phased averaging and 3-D ESPRIT for joint azimuth-elevation-carrier estimation, IEEE Trans. Signal Process. 49 (1) (2001) 54–62.
[28] C. Stoeckle, J. Munir, A. Mezghani, J.A. Nossek, DOA estimation performance and computational complexity of subspace-and compressed sensing-based methods, in: Proceedings of the 19th International ITG Workshop on Smart Antennas, March 2015, pp. 1–6.

Keyvan Aghababaiyan received his B.Sc. degree in communication Engineering from Amirkabir University of Technology of Tehran, Iran in 2011 (with highest honors) and received his M.Sc. degrees in Communication Engineering from Sharif University of Technology of Tehran, Iran in 2013. He is currently working toward the Ph.D. degree at the School of Electrical and Computer Engineering, University of Tehran, Tehran, Iran. His research interests include Nano-neural communication systems, wireless communication and adaptive antennas.

Reza Ghaderi Zefreh received the B.Sc. degree in electronic engineering from University of Isfahan, Iran, in 2012 and received the M.Sc. degrees in communication engineering from University of Tehran, Iran, in 2014. He is currently pursuing a Ph.D. degree in communication engineering at Isfahan University of Technology, Iran. His research interests include signal processing, detection, and estimation.

Vahid Shah-Mansouri received the B.Sc., M.Sc., and Ph.D. degrees in electrical engineering from the University of Tehran, in 2003, Sharif University of Technology, in 2005, and University of British Columbia, in 2011, respectively. Since 2013, he is with the Department of Electrical and Computer Engineering, University of Tehran, Iran as an Assistant Prof. His research interests include the design and mathematical modeling of communication and computer networks, heterogeneous networks, 5G core architecture and Nano-neural communication systems.